

Incremental dynamic analysis of caisson–pier interaction

A. Zafeirakos, N. Gerolymos*, V. Drosos

National Technical University of Athens, Greece

ARTICLE INFO

Article history:

Received 2 May 2012

Received in revised form

23 January 2013

Accepted 28 January 2013

ABSTRACT

This paper presents a 3D finite element Incremental Dynamic Analysis (IDA) study of caisson foundations carrying single-degree-of-freedom (SDOF) structures on clayey soil. The emphasis is given to the interplay between the nonlinearities developed above (superstructure) and, mainly, below ground surface, either of material (soil plasticity) or of geometric (caisson–soil interface gapping and slippage) origin. The study is performed with respect to the static (F_S) and the seismic (F_E) safety factor of the foundation and involves SDOF oscillators of varying mass (to account for vertical loading, F_S) and height (relating to moment loading, F_E) founded on similar rigid cubic caissons. Structural nonlinearity is considered through a simplified moment–curvature law and the yield strength is deliberately chosen so that the following three configurations are obtained: (a) a lightly loaded ($F_S=5$) seismically *under*-designed (as compared to the superstructure) caisson, (b) a lightly loaded seismically *over*-designed caisson, and (c) a heavily loaded ($F_S=2.5$) seismically *under*-designed caisson. The analysis is performed with several earthquake records, each scaled to multiple levels of intensity. IDA curves are produced for a single intensity measure, (peak ground acceleration, PGA), and appropriate engineering demand parameters (EDP) describing both the maximum and the residual response of the system. The results emphasize a potentially beneficial role of foundation nonlinearities in reducing the seismic demands on the superstructure, but at the cost of residual foundation settlements and rotations.

© 2013 Elsevier Ltd. All rights reserved.

1. Introduction

The seismic design of deeply embedded caisson foundations has been based either on solutions for shallow embedded foundation [7,8,12,26,33,35,42,43] (mostly cylindrical) or on solutions for pile (e.g. [28,41]). Gerolymos and Gazetas [16,17,18] proposed a multi-spring model for the static, cyclic, and dynamic response of massive caisson foundations embedded in nonlinear layered or inhomogeneous soil and loaded at the top, taking into account for soil and interface nonlinearities. In a recent related work, Varun et al. [47] developed a dynamic Winkler model that accounts for the multitude of soil resistance mechanisms mobilized at the base and the circumference of laterally loaded caissons, thus retaining the advantages of Winkler-type models while allowing for realistic representation of the complex soil–structure interaction effects.

Current seismic design of structures is based on the so-called “capacity design” approach, in which the structural response is presumed ductile. In essence, it dictates the hierarchy of failure, ensuring that the critical components of a joint (column/pier-to-foundation or beam-to-column), which are the foundation and the columns respectively, are not designed by their own action effects but

to exceed, by an appropriate capacity factor, the available resistance of the “sacrificial” components, the latter designed by their nominal earthquake loading coefficient. Structurally elastic behavior of the foundation, for the case of deep embedded and caisson foundations, indicates that passive and shear failure along the sides and the base are undesirable. Although such restrictions may, at first, appear reasonable (the inspection and rehabilitation of foundation damage after a strong earthquake is not a trivial task), they may lead to economically conservative designs; elastic foundation response might prove a rather expensive solution. Moreover, neglecting the aforementioned nonlinear phenomena prohibits the exploitation of the substantial ductility capacity offered by the failure mechanisms developed below ground surface in dissipating the seismic energy. In fact, recent research on shallow (e.g. [2,9,10,14,15,22,27,36,38,39]) and pile [20] foundations suggests that soil compliance and subsequent development of nonlinearities and inelasticity in the soil–foundation system may be beneficial for the superstructure and should be considered in the analysis and perhaps allowed in the design. However, the consequences of allowing for plasticity below ground surface include transient and permanent deformations which must be realistically assessed in design.

The impact of nonlinear soil–foundation–structure interaction (SFSI) on the seismic response of caisson foundations was illustrated in a recent numerical comparative study by the authors [49]. The study comprised similar rigid cubic caissons carrying elastic single

* Corresponding author. Tel.: +30 6974 782 521; fax: +30 210 772 2405.
E-mail addresses: gerolymos@gmail.com, gerolymo@mail.ntua.gr (G. N.).

degree of freedom (SDOF) structures, of varying mass and height, in clay. Four different configurations were examined, with respect to the static (F_V) and seismic (F_E) safety factor of the foundation, corresponding to lightly ($F_V=5$) and heavily loaded ($F_V=2.5$) seismically *over-* ($F_E > 1$) and *under-* ($F_E < 1$) caissons. It was shown that seismically *under-*designing a caisson foundation, thus deliberately *allowing* for plastic deformations to develop below ground level, generally leads to:

- Reduction in “floor” response and spectral accelerations.
- Significant reduction in flexural structural deformations.
- Increased dynamic settlements and rotations but minimal residual displacements and tilting.

Overall, the paper highlighted the effectiveness of interface nonlinearities, prevalent in the response of the *under-*designed foundations, in damping the seismic energy, owing to the large ductility capacity of the soil mass.

Incremental Dynamic Analysis is a tool to assess the global and local capacity of structures by subjecting the structural model to several ground motion records, each scaled to multiple levels of intensity. Though introduced and well documented by Vamvatsikos and Cornell [44], the concept of seismic load scaling had been formerly used by several authors to assess the performance of structural frames in buildings [3,31,34]. This method of analysis provides several insights regarding the dynamic characteristics of a structural system as well as useful input for applications of performance-based evaluation. In a recent relevant publication, Pecker and Chatzigogos [40] presented results of IDA for a simple bridge pier founded on stiff clay with a shallow circular foundation considering soil and geometric nonlinearities. They deduced that, on a whole, consideration of nonlinear SSI appears beneficial in drastically reducing the ductility demand in the structure, while stressing out that this positive effect is counterbalanced by larger displacement and rotation of the foundation.

In this framework, the present study further extends the investigation on the seismic response of *under-*designed caisson foundations

through 3-D IDA. Similar rigid cubic caissons under three different loading conditions, with respect to the static (F_S) and the seismic (F_E) safety factor of the foundation, are examined. Since the paper aspires to characterize the global foundation–superstructure response in performance based design terms, structural nonlinearity is also accounted for, in order to capture the complex interplay between the main sources of nonlinearities; namely those above and below ground level. The main focus, however, is on the nonlinear phenomena developed at the foundation level. Therefore, structural nonlinearity is considered through a simplified moment–curvature law. The yield strength of the columns is deliberately chosen so that the following idealized configurations are obtained: (a) a 12 m and a 46 m tall column, corresponding to a seismically *over-*designed and a seismically *under-*designed (as compared to the superstructure) foundation respectively, carrying a “light” superstructure ($F_S=5$) and (b) a 18 m tall column corresponding to a seismically *over-*designed foundation carrying a “heavy” superstructure ($F_S=2.5$). Given that IDA covers the full spectrum of the dynamic capacity of the soil–caisson–superstructure system, conclusions of more general validity are expected.

As a final remark, it should be stated that although computationally demanding and challenging, the 3D analysis was preferred to more simplified approaches, e.g. Winkler-based models, due to the fact that while the latter models are, in theory, capable of capturing any observed interface behavior, their success lies on the appropriate calibration of their parameters which, unfortunately, could not be known *a priori* for each specific case. To the authors’ best knowledge, a thorough calibration procedure for Winkler-based modeling of soil–caisson interface response is still missing in the literature.

2. Problem definition and analysis methodology

2.1. Problem definition

The studied problem is portrayed in Fig. 1: A mass-and-column structure is founded through a rigid cubic caisson of side $h=10$ m in a 20 m thick 2-layer cohesive soil stratum. The soil is considered to be undrained with $S_u=65$ kPa at the upper 6 m and

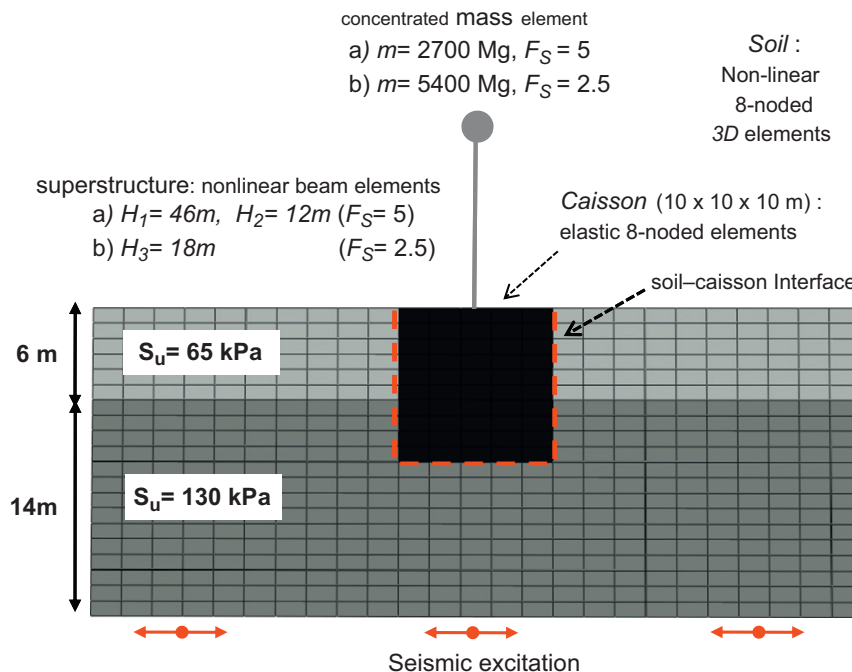


Fig. 1. Overview of the finite element model with the parameters used in the analysis.

$S_u=130$ kPa at the lower 14 m and constant stiffness to strength ratio $E/S_u=1500$. The mass-and-column superstructures are modeled as single degree of freedom (SDOF) oscillators. The concentrated oscillator mass, m , is given parametrically the values of 5400 and 2700 Mg, corresponding to a static factor of safety $F_S=2.5$ (“heavy” superstructure) and $F_S=5$ (“light” superstructure) respectively. For each case of F_S , different column heights are calculated; one for the former and two for the latter. In total, a set of three structural configurations are analyzed.

The height and strength of the superstructures are calculated according to the following two-step procedure:

with the respective contours of plastic strain magnitude at failure.

- Using the strength envelopes derived at the first step, the height of the superstructure is deliberately calculated to match a “target” critical (yielding) acceleration ($A_{c,f}$), applied at the superstructure mass level, associated with bearing capacity of the foundation. Structural yielding is then either prevented (*under-designed* foundation) or pursued (*over-designed* foundation) by designing the superstructure for a critical acceleration ratio:

$$\frac{A_{c,f}}{A_{c, str}} < 1 \tag{1}$$

or

$$\frac{A_{c,f}}{A_{c, str}} > 1 \tag{2}$$

- A series of finite element static pushover-type of analyses are carried out to derive the bearing strength surfaces of the caisson–soil system in moment (M)–horizontal load (Q) space. Two envelopes are produced, depicted in Fig. 2, one for each case of vertical load applied from the mass weight. The results are normalized with respect to the pure moment capacity M_u (with no horizontal loading) and the pure horizontal capacity Q_u (no moment loading) of the caisson–soil system. The verification of the aforementioned entities is given in Fig. 3 in terms of Q – u and M – ϑ curves along

respectively, where $A_{c, str}$ is the critical (at yield) spectral acceleration of the structure. Since the superstructure is modeled as SDOF oscillator, the horizontal force at the top of the caisson is related to the overturning moment as $M=Q \cdot H$.

It should be noted at this point that since this work comprises a theoretical study on the SFSI of the same caisson under various

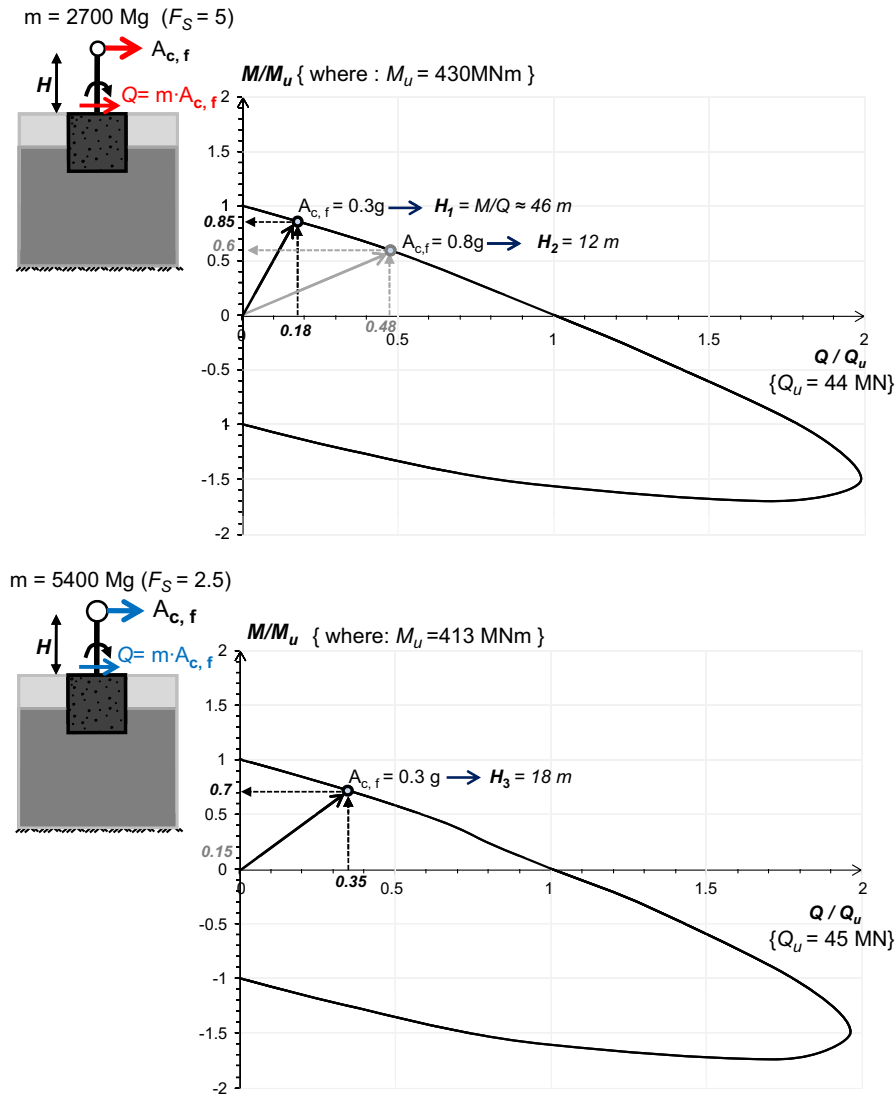


Fig. 2. Normalized M – Q interaction diagrams for $F_S=5$ (top) and $F_S=2.5$ (bottom): calculation of the column heights for the seismically *over-designed* ($A_{c,f}=0.8$ g) and *under-designed* ($A_{c,f}=0.3$ g) foundations.

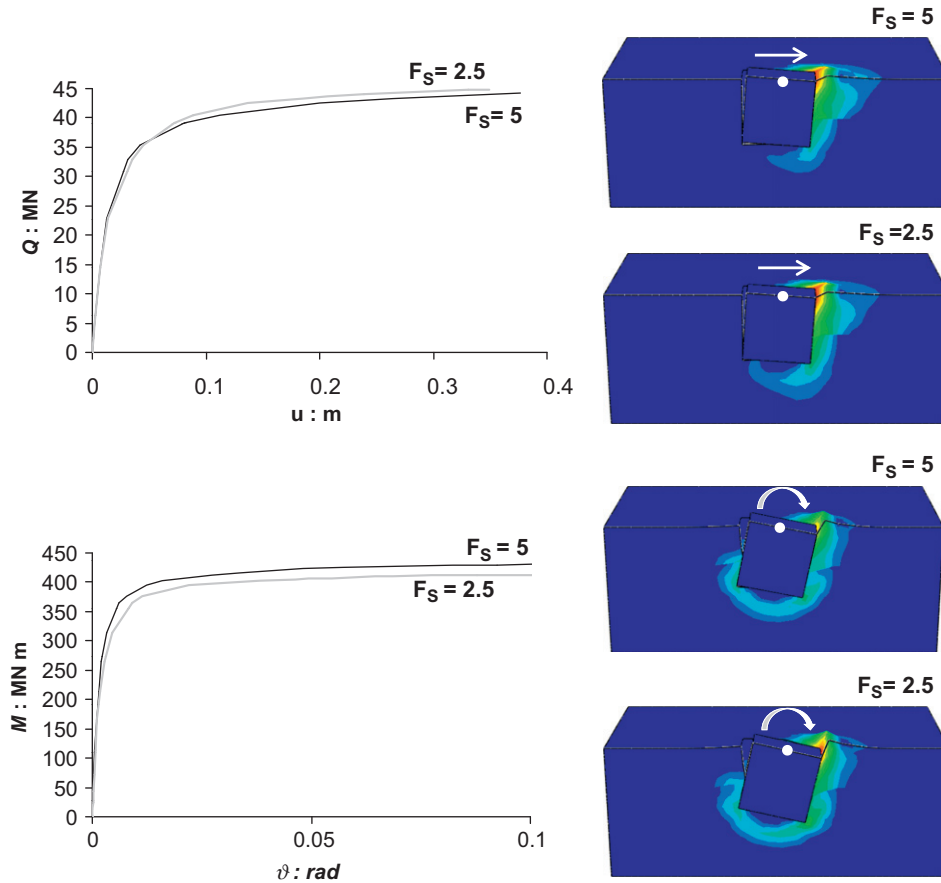


Fig. 3. $Q-u$ and $M-\theta$ curves corresponding to monotonic loading at the top of the caisson along with the respective contours of plastic strain magnitude at failure, for $F_S=5$ and $F_S=2.5$.

loading cases and does not intend to propose specific design guidelines, any value of $A_{C,f}$ that stems from the strength envelopes and any value of $A_{C,str}$ that satisfies condition (1) or (2), should suffice for our parametric study. In this paper, values for $A_{C,f}$ and $A_{C,str}$ are arbitrarily chosen so that the critical acceleration ratio, r_{max} , defined as

$$r_{max} = \frac{\max\{A_{C,f}, A_{C,str}\}}{\min\{A_{C,f}, A_{C,str}\}} \quad (3)$$

is kept constant for all cases considered. Assuming $A_{C,f}=0.3$ g and $A_{C,str}=0.8$ g for the seismically *under*-designed caissons, (3) leads to $A_{C,f}=0.8$ g and $A_{C,str}=0.3$ g for the seismically *over*-designed caisson.

Fig. 2 schematically illustrates the process for calculating the column heights for both the seismically *over*- and *under*-designed foundations. The three model configurations are summarized in Table 1:

2.2. Numerical modeling aspects

The problem is analyzed with the finite element code ABAQUS (Fig. 4). Both caisson and soil are modeled with 3D 8-noded solid elements, assuming elastic behavior for the former and nonlinear for the latter. The superstructure is modeled with 3D nonlinear Timoshenko beam elements. The caisson is connected to the soil with special contact surfaces, allowing for realistic simulation of the possible detachment and sliding at the soil-caisson interfaces. The mesh for the soil-caisson consists of 12 500 elements. The analyses were performed in a Core i-7 desktop processor, 2.8 GHz and 8 GB RAM. Depending on the severity of the input seismic motion, each analysis lasted approximately 16–24 h. To improve

Table 1 Summary of the model configurations used for the dynamic analysis.

Model	m (Mg)	F_S	H (m)	A_c : critical spectral acceleration	Foundation
1	2700	5.0	46	0.3 g (foundation) 0.8 g (superstructure)	<i>Under</i> -designed
2	2700	5.0	12	0.8 g (foundation) 0.3 g (superstructure)	<i>Over</i> -designed
3	5400	2.5	18	0.3 g (foundation) 0.8 g (superstructure)	<i>Under</i> -designed

the computational cost without jeopardizing the accuracy of the analysis, the surface-to-surface contact interaction was modeled by exponential (“softened”) pressure-overclosure relationship through the direct constraint enforcement method that makes use of Lagrange multipliers. For more details on the contact interaction algorithm the reader is referred to ABAQUS manual [1].

The location and type of lateral boundaries is an important consideration in the dynamic modeling. It is known from the literature that whereas under monotonic and cyclic static loading these boundaries can be placed fairly close to the foundation (just outside the “pressure bulb”) and they can be of any “elementary” type (from “free” to “fixed”), under dynamic loading waves emanating from the footing-soil interface cannot propagate to infinity unless special transmitting boundaries are placed at suitably large distances. “Elementary” boundaries may cause spurious reflections, thereby contaminating the wave field below the foundation and reducing or even eliminating the radiation damping. In this particular case, however, even “elementary”

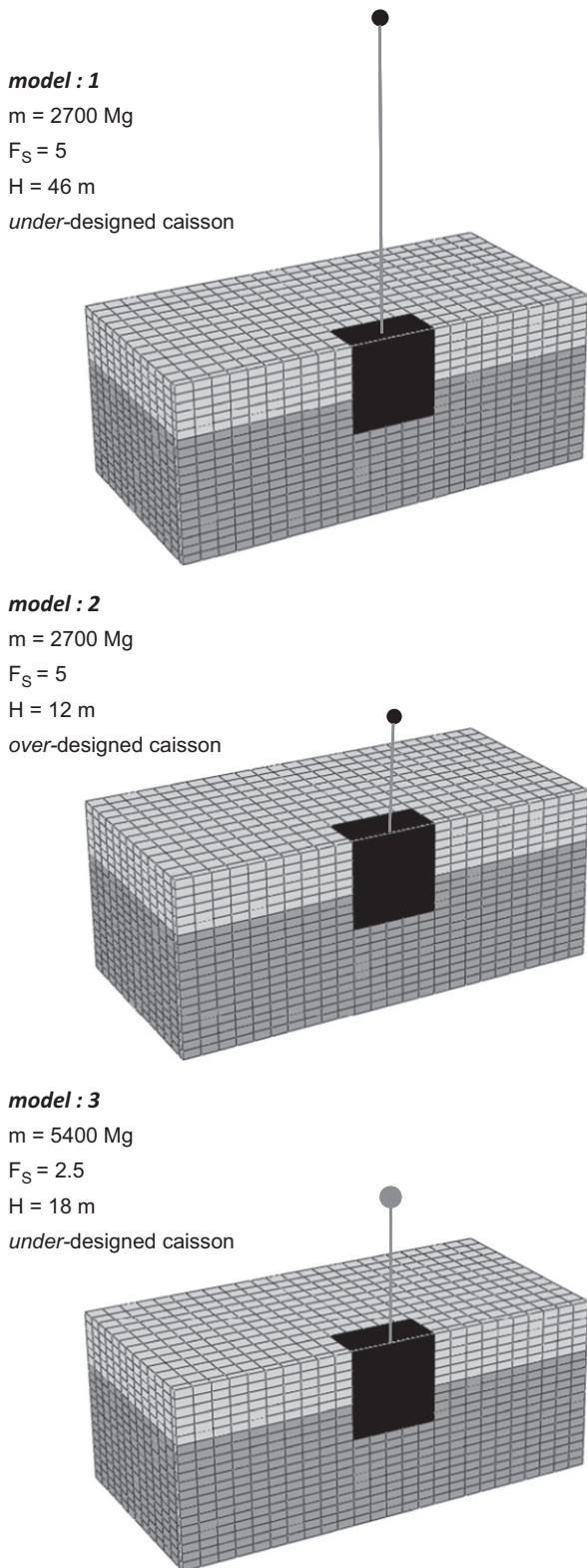


Fig. 4. Finite element discretization of the three configurations analyzed (column heights not in scale).

boundaries placed at a “reasonably large” distance from the foundation might suffice, for the following reasons:

1. Under low frequency dynamic loading, waves emitted from symmetrically opposite points of the foundation contact

surface, being out-of-phase, “interfere destructively” and thus limit substantially the radiation of wave energy [13,25,30,48]. Therefore, even in an (infinite) halfspace, boundaries placed at short distances from the loaded surface would hardly be “seen” by the waves emitted from the caisson.

2. The geometric properties of the superstructures were appropriately calculated so that the elastic fixed-base period $T_{str}=0.6 \text{ s}$, for all cases, is deliberately larger than the first natural period, $T=0.41 \text{ s}$, of the soil profile. In this way spurious reflections at the boundaries of the model are limited as a result of a destructive interference (existence of a cut-off period for radiation damping equal to the first natural period of the soil profile) of the outward spreading waves [12,13]. “Elementary” boundaries placed at relatively short distances (a few widths) would therefore suffice.
3. In most cases analyzed, soil inelasticity is activated, mobilizing bearing capacity failure mechanisms. The presence of the associated localized failure surfaces (at small distances from the caisson) has the effect of creating a softer zone inside the (stiffer) soil; this zone would reflect the incident waves, thus further reducing the amount of wave energy transmitted (“leaking”) into the surrounding soil. Borja et al. [4,5] thoroughly examined the aforementioned phenomenon for the case of surface footings.

In the absence of a cut-off frequency for the radiation damping, then the “elementary” boundaries should be placed at far distances from the loaded surface, e.g. at approximately $L=10 \text{ B}$ [37], increasing prohibitively the computational cost. The use of appropriate wave energy transmitting boundaries would alleviate the cost of analysis even if placed at relatively short distances. However, to the authors’ knowledge, special boundaries that can absorb accurately all types of body and surface waves at all angles of incidence and all frequencies, consistent with a predefined acceleration time history (input motion) at the base of the model, does not exist in the literature.

A distance of $L=5 \text{ B}$ was therefore adopted in all studied cases. Moreover, appropriate kinematic constraints are imposed to the lateral edges of the model, allowing it to move in horizontal shear as the free field [19,21]. The nodes at the bottom of the finite element mesh are fixed in the vertical direction and they follow the horizontal motion imposed by the seismic records.

2.3. Constitutive modeling

2.3.1. Soil

For the total stress analysis under undrained conditions soil behavior is modeled through a nonlinear constitutive law [18] which is a slight modification of one incorporated in ABAQUS. It uses the Von Mises failure criterion with yield stress σ_y related to the undrained shear strength S_u as

$$\sigma_y = \sqrt{3} \cdot S_u \quad (4)$$

along with a nonlinear kinematic and isotropic hardening law, and an associative plastic flow rule. The model parameters are calibrated to fit published $G-\gamma$ curves of the literature. Fig. 5(a) and (b) illustrates the validation of the kinematic hardening model (through simple shear finite element analysis) against published $G-\gamma$ and $\xi-\gamma$ curves by Ishibashi and Zhang [24]. Mass and stiffness proportional Rayleigh damping, representing material damping, are taken equal to 5% between the eigenfrequency of the soil deposit and the dominant frequency of the earthquake ground motion.

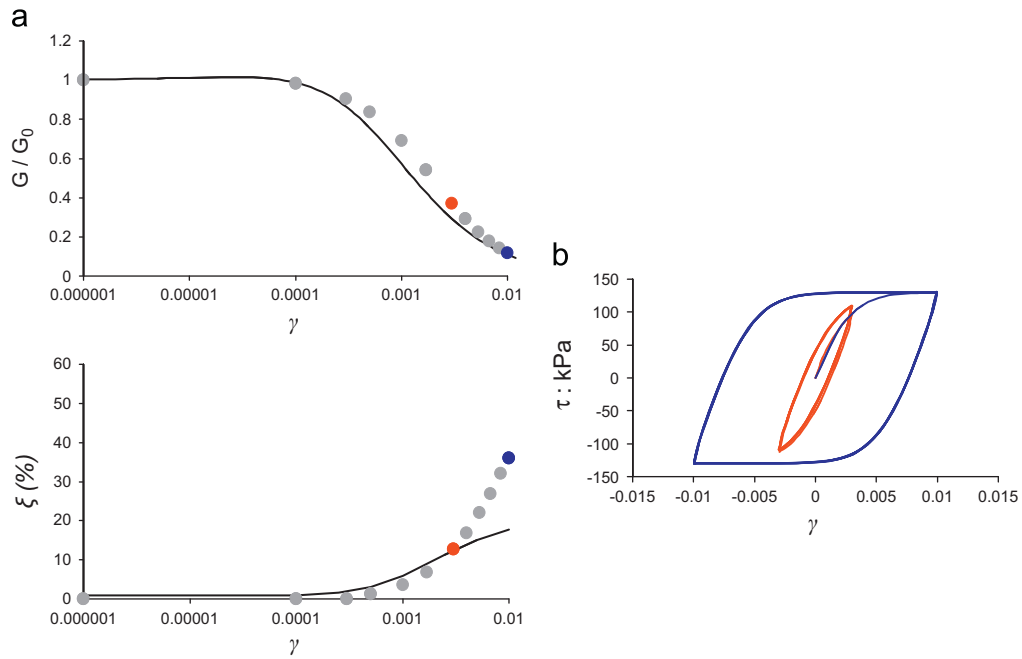


Fig. 5. (a) Calibration of kinematic hardening model for soil (stiff clay, $S_u = 130$ kPa, $G_0 = 500S_u$) against published $G-\gamma$ and $\xi-\gamma$ ($PI=30$, $\sigma_v = 200$ kPa) curves (Ishibashi and Zhang, 1993). (b) Shear stress–strain loops corresponding to the designated points in (a).

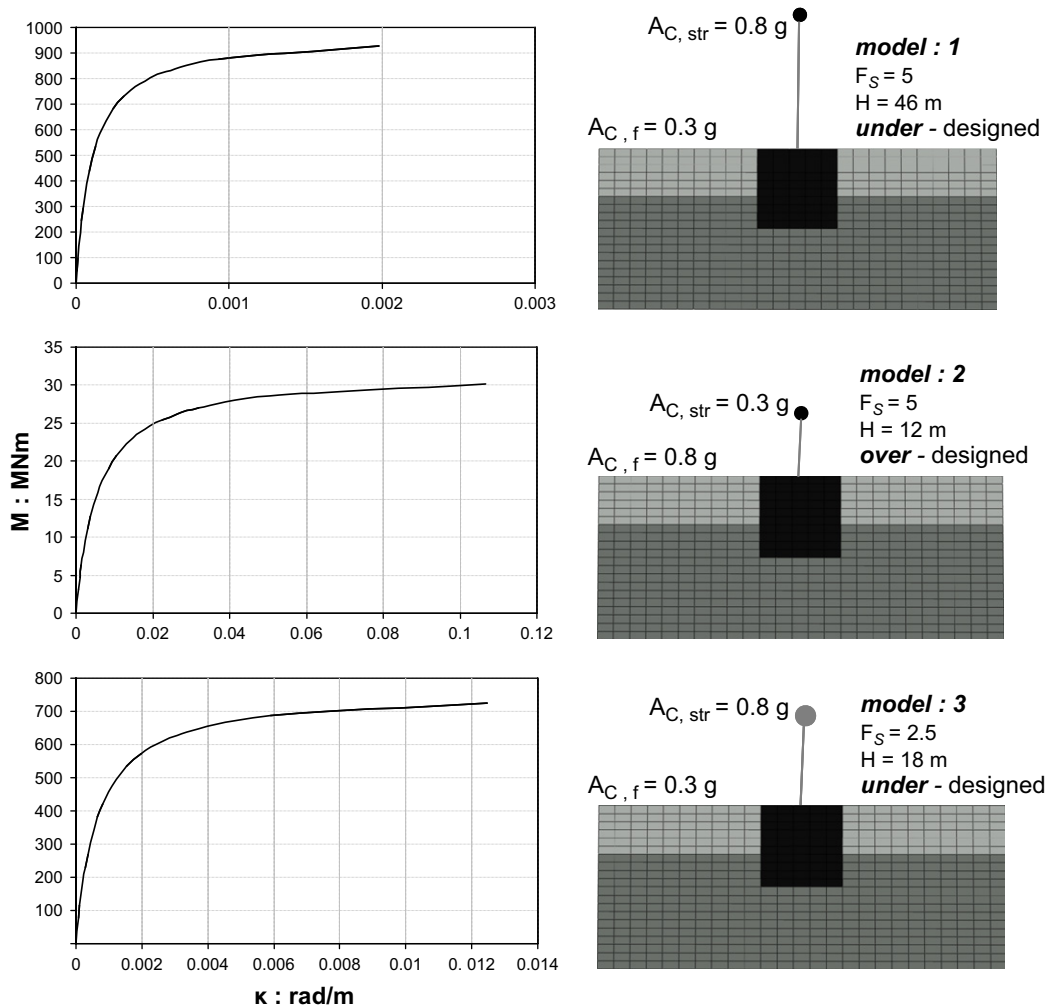


Fig. 6. Predefined moment-curvature relations used for superstructure inelasticity (column heights not in scale).

2.3.2. Superstructure

In their previous work the authors considered elastic superstructures, thus focusing solely on the role of soil and interface nonlinearities in the response. However, as aforementioned, the engineering motivation of this paper has arisen from the recent developments of performance based design approaches, which aim at characterizing the structural behavior in terms of displacement, rotation, distortion and drift rather than in terms of strength criteria. Since both superstructure and soil–foundation can be potential sources of nonlinearities and energy dissipation during a strong earthquake, they should be both characterized by nonlinear models, allowing to capture their complex nonlinear interplay, and giving a reliable estimate of system deformation, both at the foundation and the superstructure level [6,9]. Therefore, structural nonlinearity is introduced. A simple hyperbolic backbone moment (M)–curvature (κ) curve describes this nonlinear behavior of the column:

$$\kappa = \frac{M_y}{EI} \cdot \left(\frac{M}{M_y - M} \right) \quad \text{for } M < M_y \quad (5)$$

where EI is the initial structural bending stiffness and M_y is the bending moment yield strength associated with the critical

acceleration ($A_{C, str}$). Fig. 6 shows the respective nonlinear M – κ curves of the examined systems. Regarding the elastic fixed-base period ($T_{str}=0.6$ s) of the columns, the choice was deliberate so the comparison of their effective response, namely the T_{SSI} , is performed on a *fair* basis; that is from the same starting point. Furthermore, given that the determination of shear strength and especially of shear deformation characteristics of (e.g. reinforced concrete) structures are still controversial issues [32], the interplay between shear and flexure in the inelastic regime is not taken into account and the controlled mode of failure is assumed to be flexure-dominated.

3. Static pushover analysis

Prior to the dynamic analysis, we investigate the response in terms of monotonic loading: the static “pushover” test. Displacement controlled horizontal loading is applied atop the superstructure mass. To investigate the level of nonlinear SSI effects developed in the seismically *over-* and *under-*designed caissons, the tests involved: (a) fixed-base superstructures (no SSI effects) and (b) complete soil–structural models considering

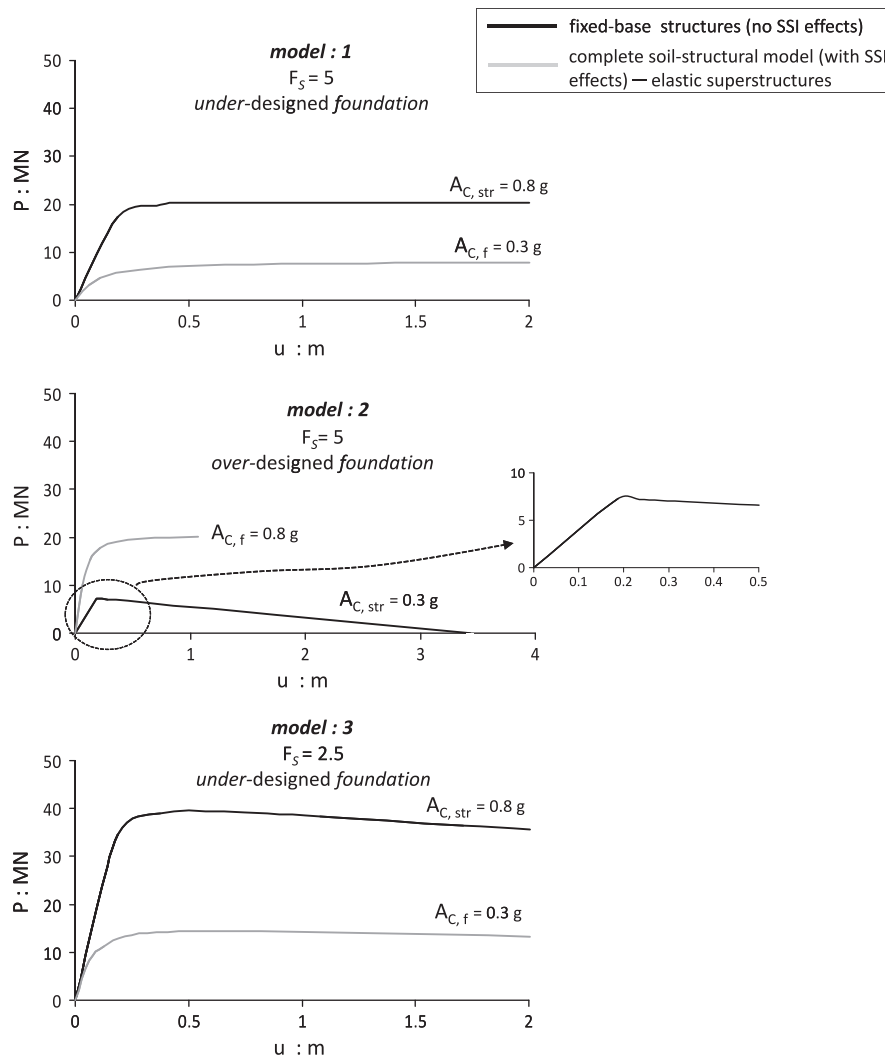


Fig. 7. Load–displacement pushover curves for horizontal loading of all examined systems.

elastic superstructures, in order to determine the pure lateral capacity of the caisson. As illustrated in Fig. 7, in terms of load–displacement relation at the structure mass, SSI effects are virtually absent in the seismically *over*-designed foundation (*model 2*), where structural inelasticity governs entirely the system response. Notice the negative slope of the force–displacement curve, attributed to P – δ effects and not to stiffness degradation of the material of the superstructure. Structural

collapse occurs when the curve reaches the point of zero horizontal load. It can be observed, however, that the aforementioned behavior, also qualitatively similar to the results by Hutchinson et al. [23] and Lignos et al. [29], becomes prevalent at rather large displacements. In stark contrast, plasticity that developed below ground level in the seismically *under*-designed foundations (*models 1 and 3*), reduces significantly the structural demand, by approximately 30% in *model 1* and 50% in *model 3*.

Table 2
Selected records for incremental dynamic analysis.

No	Event	Year	Station	Component	Soil ^a	M_w	R^b (km)	PGA (g)	CAV	Arias intensity (m/s)
1	Aegion	1995	Aegion-rock	–	A	6.1	8	0.359	247.449	0.517
2	Chi-Chi	1999	TCU	68°	C,D	7.6	0.2	0.353	1599.58	3.018
3	Kocaeli	1999	Duzce	180°	D	7.2	9	0.312	1257.38	2.654
4	Imperial Valley	1979	El Centro #4	140°	C,D	6.6	28	0.485	658.099	1.301
5	Kobe	1995	JMA	000°	B	6.9	2	0.83	1943.28	8.358
6	Kalamata	1986	Nomarxia	EW	C	6	4	0.24	367.488	0.554
7	Lefkada	2003	Hospital	W325N	C	6.4	8	0.426	1460.91	3.972
8	Northridge	1994	Rinaldi	228°	B	6.7	5	0.837	1464.88	7.156
9	Kocaeli	1999	Sakarya	EW	B	7.2	3	0.24	560.733	0.612
10	Kobe	1995	Takatori	000°	D	6.9	4	0.611	2317.8	8.592

^a USGS, Geomatrix soil class.

^b Closest distance to fault rupture.

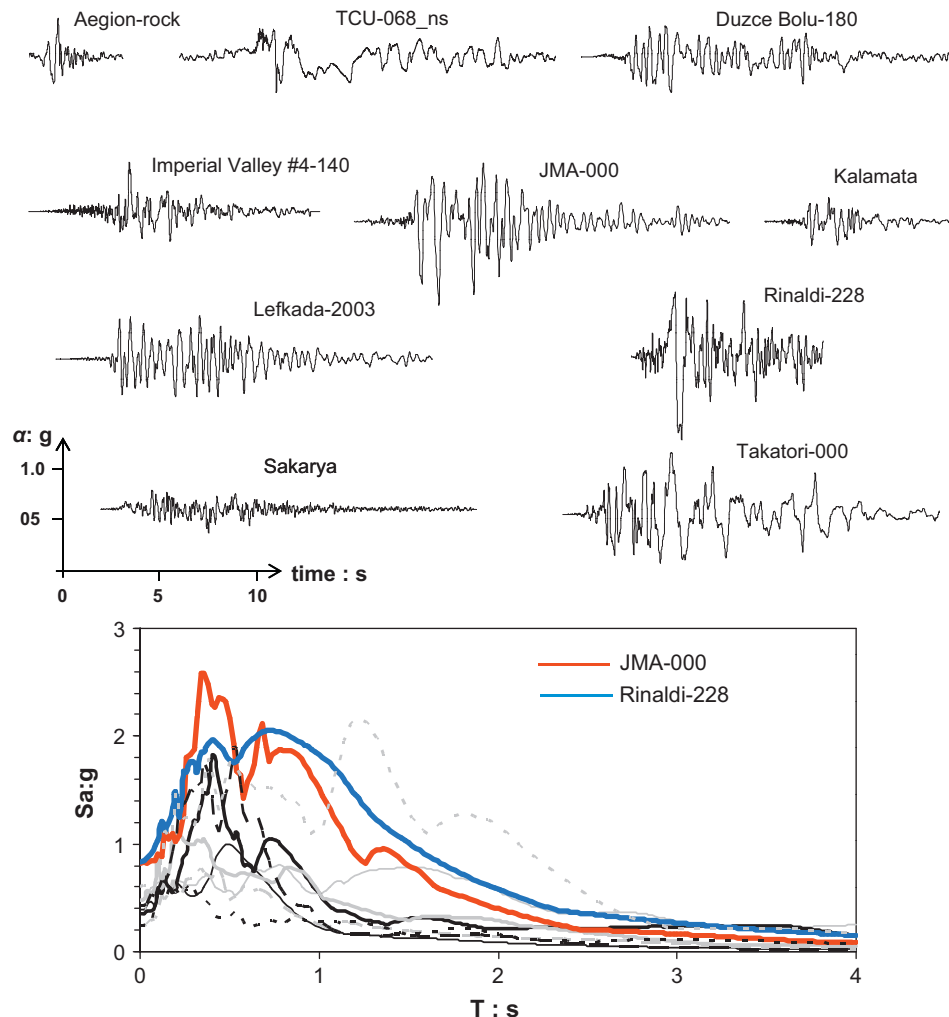


Fig. 8. Real earthquake records used for the analysis, along with their elastic spectra.

4. Incremental dynamic analysis

Incremental Dynamic Analysis (IDA) offers thorough seismic demand and capacity prediction capability [44,45]. A series of nonlinear dynamic analyses is conducted using a scaled ensemble of ground motion records, aiming at covering the entire range of response, from elasticity to collapse, having selected an Intensity Measure (IM), to represent the seismic intensity and proper Engineering Demand Parameters (EDPs) to characterize the structural response. The output is a plot of a selected IM versus a selected EDP. Similarly, an IDA curve set is a collection of IDA curves of the same structural model under different records that have been parameterized on the same IM. While each curve, given the soil–structure model and the ground motion record, is a completely defined deterministic entity, a probabilistic characterization can be brought into play by defining the 16%, 50% and 84% probability level curves (fractiles) for each IDA curve set, displaying the evolution of the effectiveness (median values) and efficiency (dispersion) of the analysis methodology.

4.1. Record suite

An ensemble of 10 real acceleration time histories has been chosen for the incremental dynamic analyses. The seismic records are imposed in a single horizontal direction at the base (“within” motion) of the finite element models. In terms of severity, the selection ranges from medium intensity (e.g. Kalamata, Aegion) to stronger (e.g. Lefkada-2003, Imperial Valley), and to very strong accelerograms characterized by forward-rupture directivity effects, or large number of significant cycles, or fling-step effects (e.g. Takatori, JMA, TCU). Note that since the scope of this study was to examine the nonlinear response of the caisson foundations in a wide range of exciting intensities, frequencies, and kinematic characteristics, selection criteria that are commonly used in the design of actual projects, such as specific soil class, magnitude, source-to-site distance R , duration, etc., were not applied.

The unscaled records are outlined in Table 2 and given along with the corresponding elastic response spectra in Fig. 8.

The scaling of the 10 real records was performed with due consideration on the role of the soil on the response of the caisson, which is two-fold:

1. It acts as a medium that amplifies (or de-amplifies) the seismic load and transmit it into the foundation. Most certainly, very strong motions may lead to soil failure during the nonlinear wave propagation prior to any possible failure of the foundation–superstructure system; a clear deviation from the scope of this work.
2. It offers the resistance mechanisms that contribute to the bearing capacity of the caisson.

In an effort to reduce the number of parameters that affect the response of the studied systems, only the second property of the foundation soil is taken into consideration. The effect of soil amplification has been deliberately eliminated by predetermining the input motion at surface level through 1-D deconvolution analysis. More specifically, all accelerograms were deconvoluted to the base of the model so that five target PGA values of free-field motion, namely 0.1 g, 0.2 g, 0.3 g, 0.4 g and 0.6 g, are calculated at the top of the soil profile. In total, 200 dynamic analyses were performed. The authors concluded that by limiting the scaling of the records to the specific five PGA values at the free-field: (a) the total computational cost is significantly reduced, while (b) gaining a clear insight into the physical phenomenon.

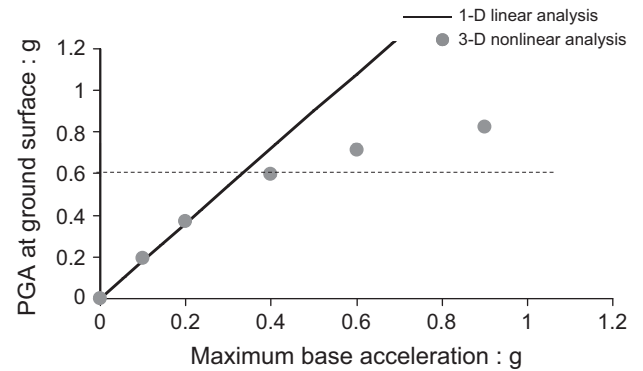


Fig. 9. Computed PGA at ground surface versus the maximum base acceleration, through 1-D linear and 3-D nonlinear analysis. Excitation: TCU-068_ns.

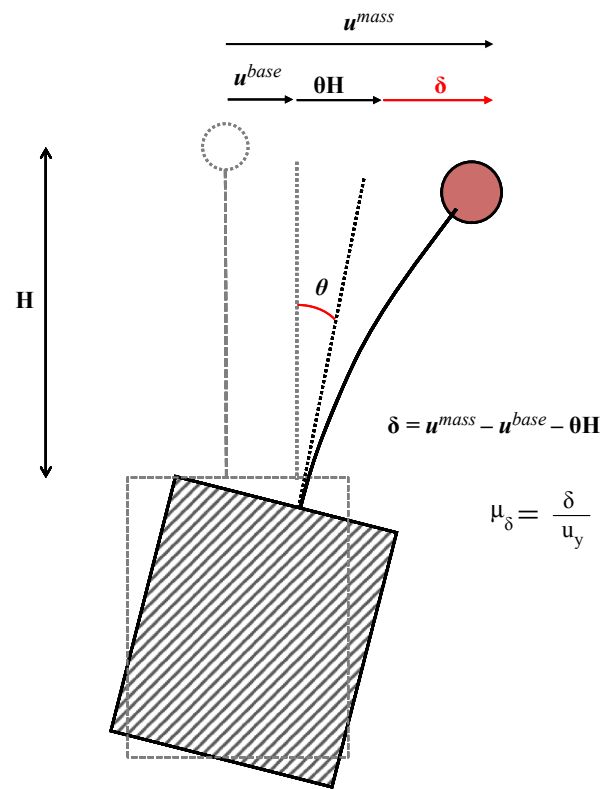


Fig. 10. Definition of the global displacement ductility demand, μ_δ .

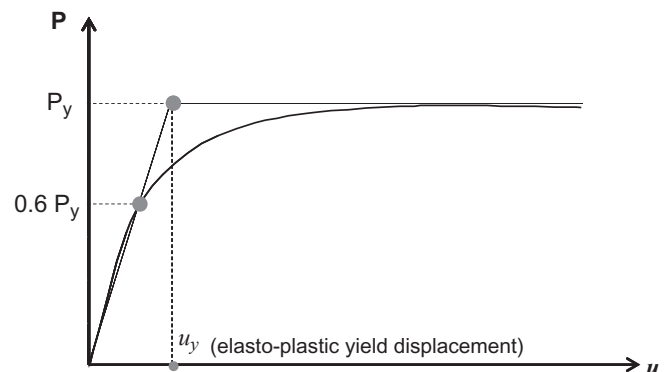


Fig. 11. Definition of yield displacement of the soil–caisson–structure system.

To elaborate on this argument, Fig. 9 compares the PGA at ground surface as a function of the maximum input acceleration at the base of the model computed through 1-D linear and 3-D nonlinear analysis, for the TCU-068 ns record. At low to moderate base acceleration levels (less than about 0.3 g) soil nonlinearity has an insignificant effect on the soil response. At higher base acceleration levels, however, there is a significant de-amplification of the ground accelerations compared to linear response analysis. Observe that the effect of nonlinearity becomes prominent for PGAs larger than 0.4–0.6 g. Therefore, to avoid excessive soil inelasticity (or even soil failure) due to seismic wave propagation, the maximum input PGA was set equal to 0.6 g.

The IDA curves, however, were based on the actually computed PGA values and not on the targeted ones. The deconvolution technique was used as a crude approximation of the PGA at the surface and the deviation from the targeted values was certainly not a restriction in our methodology.

Admittedly, simply scaling an acceleration time history to various PGA values representing the severity of an earthquake is not necessarily correct. Obviously, this is not the case for Aegion record which can be satisfactorily approximated by a single sinusoidal pulse.

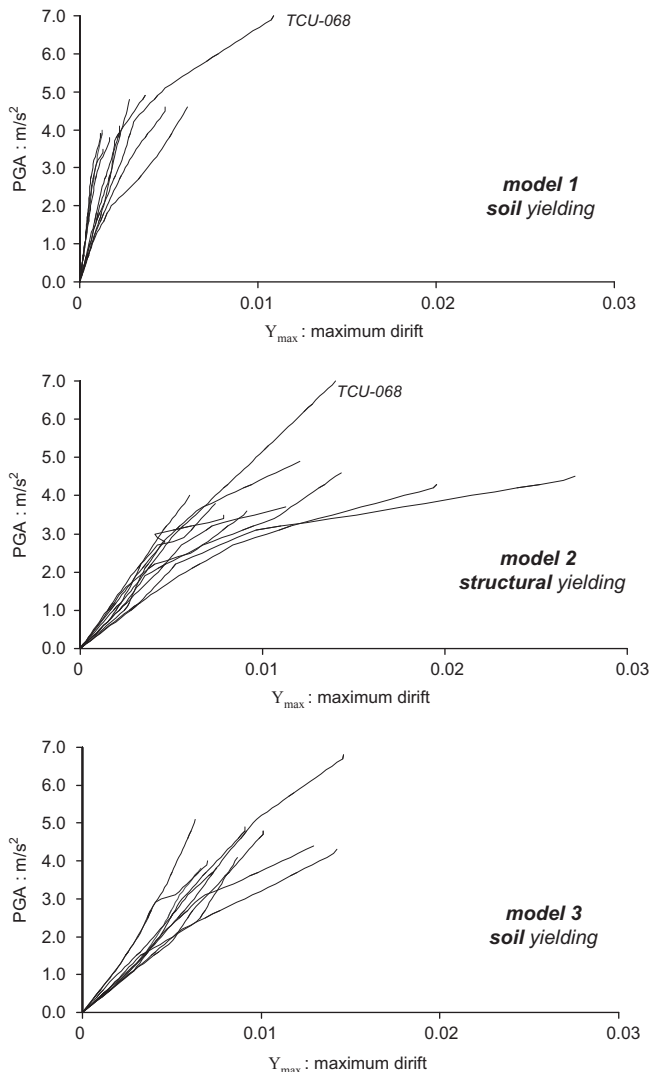


Fig. 12. IDA curves: Y_{max} (maximum drift) versus the free-field PGA for the three models.

4.2. Intensity measure

Different options are available for the IM to be used in the IDA curves. In this paper, however, a single convenient IM is used, PGA of ground surface motion. Though the PGA is among those exhibiting the less satisfactory statistical correlation with the EDPs [11], in this study it was considered as the most appropriate intensity measure, since the analyses were performed with records deconvoluted to a specific PGA at the surface of the free-field. Furthermore, it still remains the most commonly used parameter in the seismic codes for describing earthquake hazard and seismic loading.

4.3. Engineering demand parameters

Selecting an EDP is application-specific; for example, the peak floor accelerations are correlated with damage to contents and other non-structural elements damage. The maximum drift ratio, Y_{max} , is known to relate well to global dynamic instability and

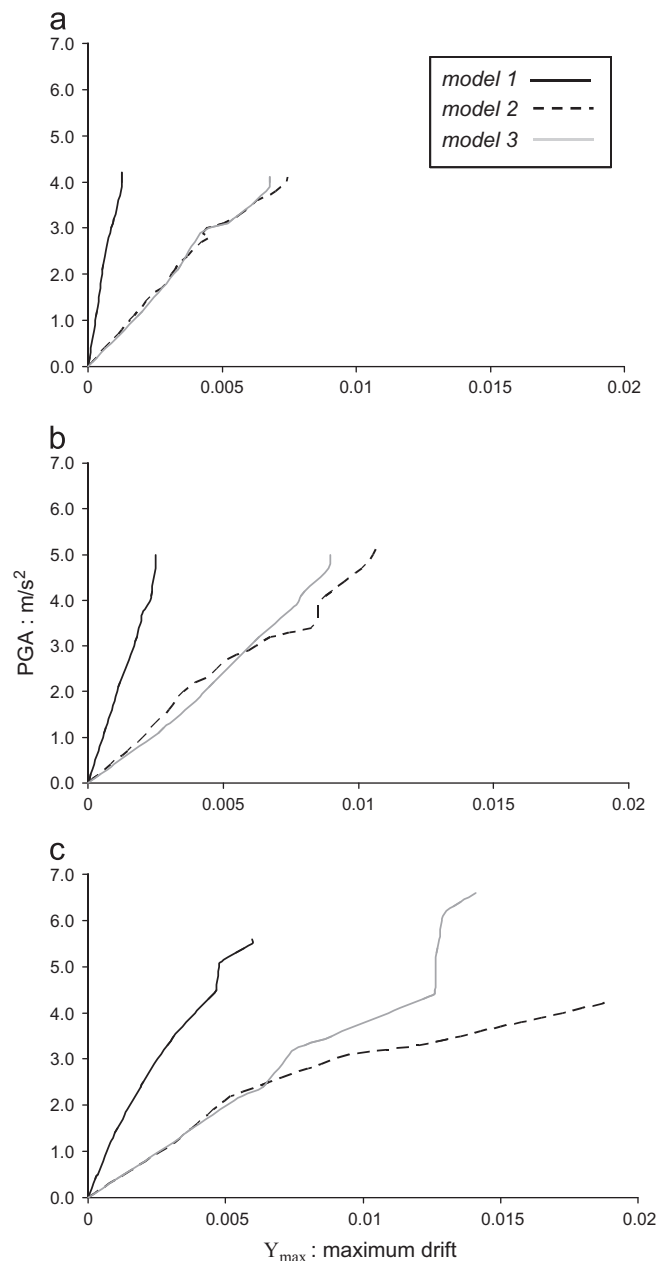


Fig. 13. Summarized IDA curves: Y_{max} (maximum drift) for the three models: (a) 16% fractiles, (b) 50% fractiles, (c) 84% fractiles.

several structural performance limit-states upon which we intend to focus [45,46]. In this paper, the following EDPs are considered:

- The maximum total horizontal drift of the oscillator, Y_{\max}

$$Y_{\max} = \max \left[\frac{u^{\text{mass}} - u^{\text{structure base}}}{H} \right] \quad (6)$$

- The maximum ductility demand: μ_{δ} .

The global (displacement) ductility demand, μ_{δ} , including the SSI effects, is the maximum ratio of the induced flexural distortion of the superstructure (free of any rigid-body motion) divided by a characteristic displacement, designated as yield displacement, u_y :

$$\mu_{\delta} = \max \left[\frac{u^{\text{mass}} - (u^{\text{structure base}} + \theta H)}{u_y} \right] \quad (7)$$

where as schematically depicted in Fig. 10, θ is the caisson rotation and H the structure height. The yield displacement u_y is assessed through the static pushover analyses of the systems, considering fixed-base structures, according to the following procedure, also

adopted by Gerolymos et al. [20]: At the mass of the superstructure, a horizontal load is progressively applied and the load–displacement curve ($P-u$) is calculated. Then, the $P-u$ curve is approximated by an equivalent bilinear elastic–perfectly plastic curve, in which the linear section is defined as the secant line corresponding to 60% of the maximum horizontal load (P_y) and the second section by the tangent line on the post-yielding section of the load–displacement curve. The intersection of these two lines defines the yield displacement u_y (Fig. 11).

- The maximum caisson rotation, θ_{\max} .
- The residual caisson rotation, θ_{res} .

Since both θ_{res} and θ_{\max} are strongly associated with phenomena such as separation and slippage between soil–caisson interface and caisson base uplifting (geometric nonlinearities), greater values are expected for the *under-designed* foundations (*models 1 and 3*).

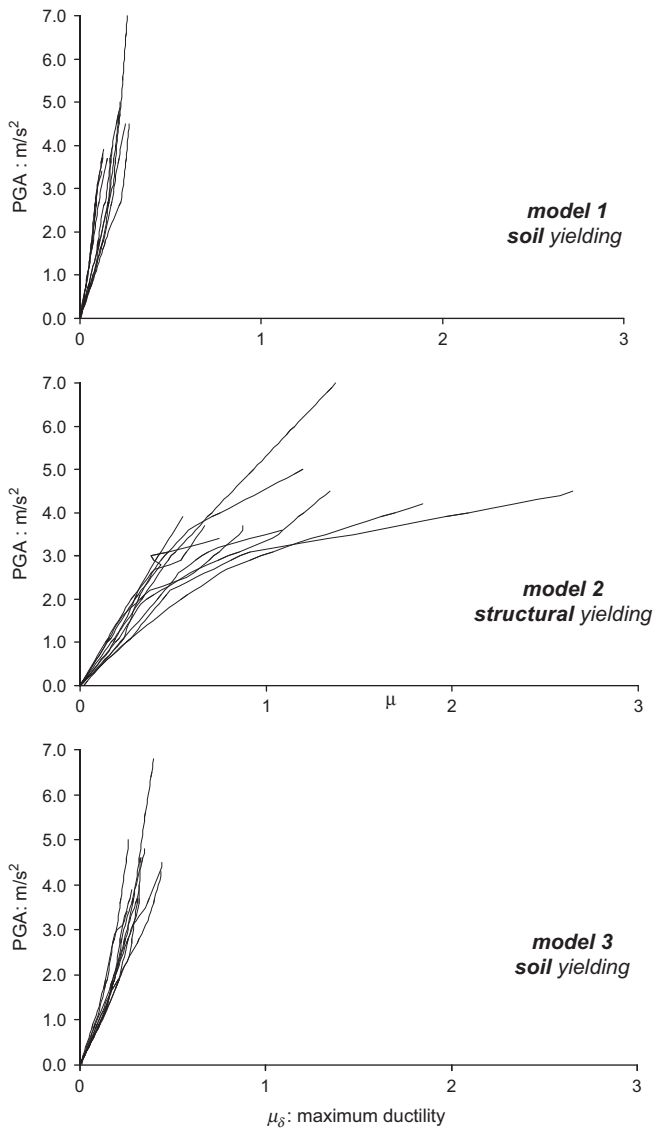


Fig. 14. IDA curves: μ_{δ} (maximum ductility) versus the free-field PGA for the three models.

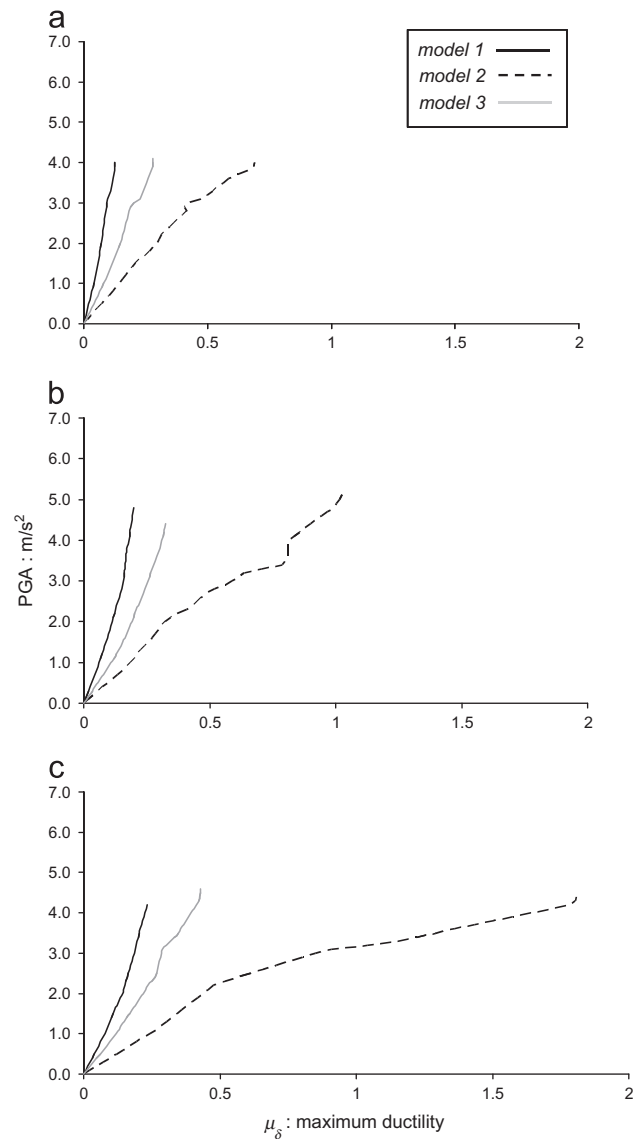


Fig. 15. Summarized IDA curves : μ_{δ} (maximum ductility) for the three models: (a) 16% fractiles, (b) 50% fractiles, (c) 84% fractiles.

5. Analysis: results and discussion

Figs. 12–19 compare the performance of all three examined systems through the IDA curves. To assist in the interpretation of these graphs, the respective 16%, 50% and 84% fractile curves are given alongside each curve set. The IDA curves were approximated by spline interpolation, while the fractile curves were derived considering the available EDP values corresponding to each IM value. The calculation process is terminated when the number of available curves corresponding to the specific IM is

- less than 9 for the 16% fractiles;
- less than 5 for the 50% fractiles;
- less than 2 for the 84% fractiles.

At first, to facilitate the understanding and explanation of results, it is fruitful to give a brief description of the mobilized impedance mechanisms that govern the response of the studied systems [49]. That is

- (a) Soil inelasticity and bearing capacity failure mobilization that generate hysteretic damping. This type of impedance mechanism dominates the response of *over-designed* foundations.
- (b) Radiation damping due to the outward—emitted from the caisson–soil interface—spreading waves (only marginal in our case due to the existence of a cut-off period).

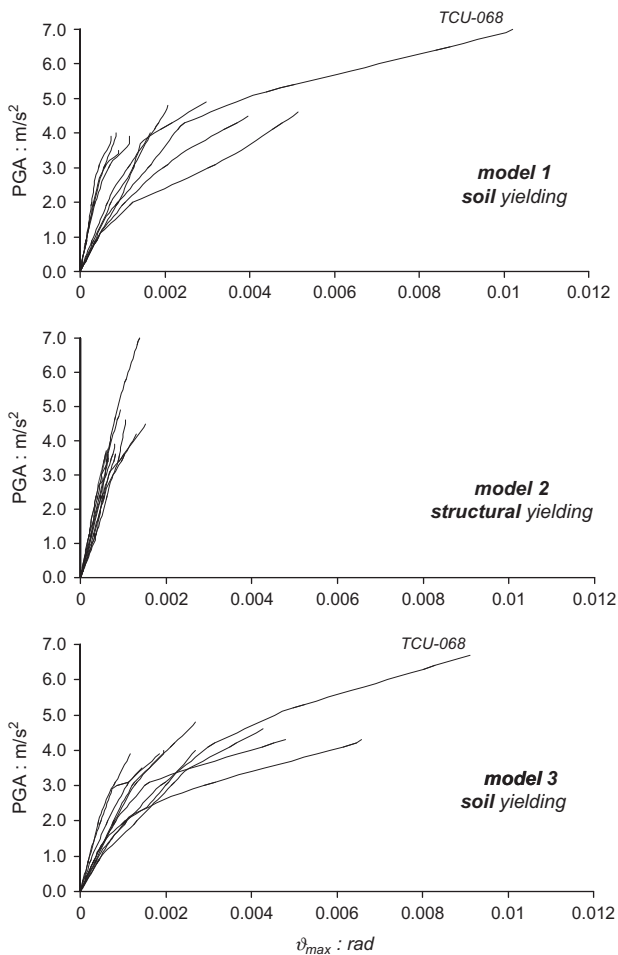


Fig. 16. IDA curves : ϑ_{max} (maximum caisson rotation) versus the free-field PGA for the three models.

- (c) Geometric nonlinearities: uplift and sliding at the caisson–soil interfaces that lead to a threshold value (*cut-off*) for the maximum transmitted seismic forces. This type of impedance mechanism is the most influential one to the response of the *under-designed* foundations.

The IDA curves for the maximum horizontal drift, Y_{max} , a measure of structural distress, are given in Fig. 12 and the corresponding fractile-specific curves in Fig. 13. Interestingly, the lightly loaded systems (*models 1 and 2*) exhibit a quite similar response with the *under-designed* heavily loaded foundation (*model 3*) and especially *model 2* ($F_S=5$, *over-designed* caisson) and *model 3*. Undoubtedly, however, the most advantageous response concerning structural demand is exhibited by the *under-designed* lightly loaded *model 1*. The latter exhibits minimal drift—a clear evidence of the beneficial geometric nonlinearities governing the response.

At this point the following remarks should be made:

- Concerning the scaled record suite, observe that no seismic record, with the exception of one, produces PGA at the

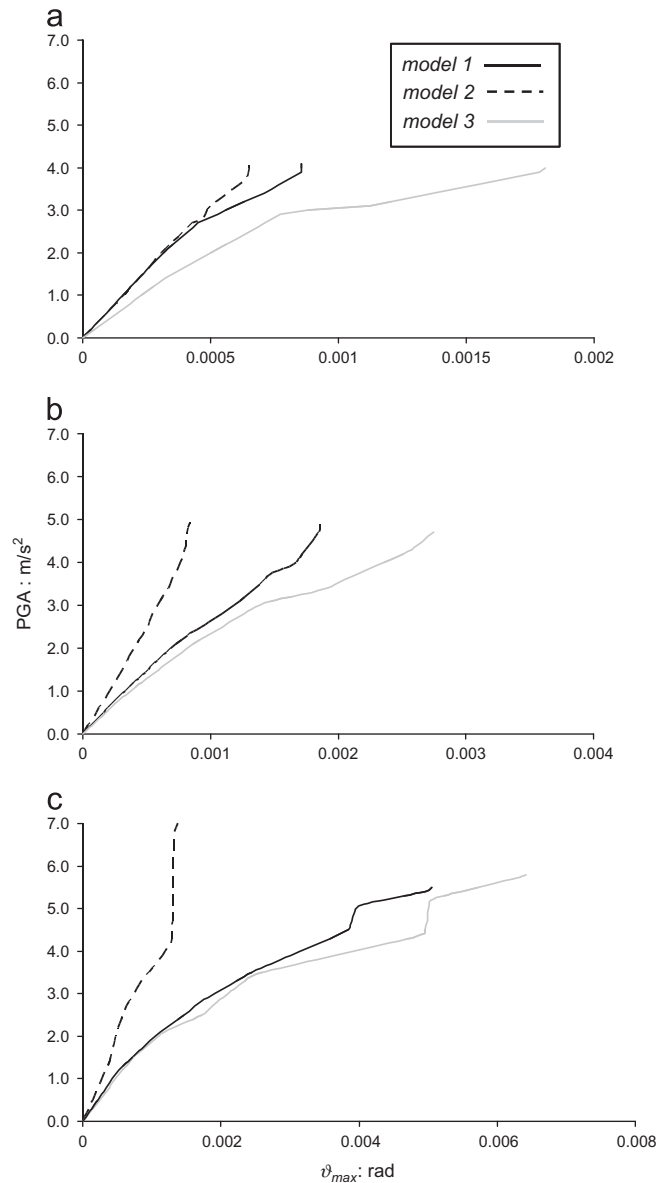


Fig. 17. Summarized IDA curves : ϑ_{max} (maximum caisson rotation) for the three models: (a) 16% fractiles, (b) 50% fractiles, (c) 84% fractiles.

free-field greater than 0.6 g. The remarkable TCU-068 record (from Chi-Chi, 1999), however, proves the severity of the near-fault ground motions bearing fling-step, by reaching 0.71 g after propagating through the nonlinear soil stratum, even though scaled for 0.6 g in a 1-D equivalent linear analysis. It is furthermore obvious that the *IM* used in the analyses (PGA at the free-field) cannot be predicted *a priori*.

- Note that from the analyses no ‘flatlines’ [44–46] were produced, which would indicate a rapid increase of the EDP towards ‘infinite’ values for small changes in the *IM*, thus signaling global dynamic instability. The explanation lies in the definition of the problem and the selection of the *IM*, since, as justified previously, the maximum PGA at the free-field to which the seismic records were scaled was 0.6 g.
- The aforementioned observations may explain why in this study the widely used tracing algorithms, such as the *Hunt & Fill* or the *constant IM-step* algorithms [45,46] could not be implemented for the generation of the IDA curves.

The IDA curves for the maximum displacement ductility demand (μ_δ) are portrayed in Figs. 14 and 15. Once more, the beneficial influence of geometric nonlinearities, dominant in the response of the seismically *under-designed* foundations (*models* 1 and 3), on the distress of the superstructure is evident. While the *over-designed model 2* exhibits ductility demands $\mu_\delta \geq 1$ for most of the seismic motions, the respective demand on the columns founded on the *under-designed* caissons is $\mu_\delta \leq 1$. This may be attributed to the fact that although the *over-designed* caisson

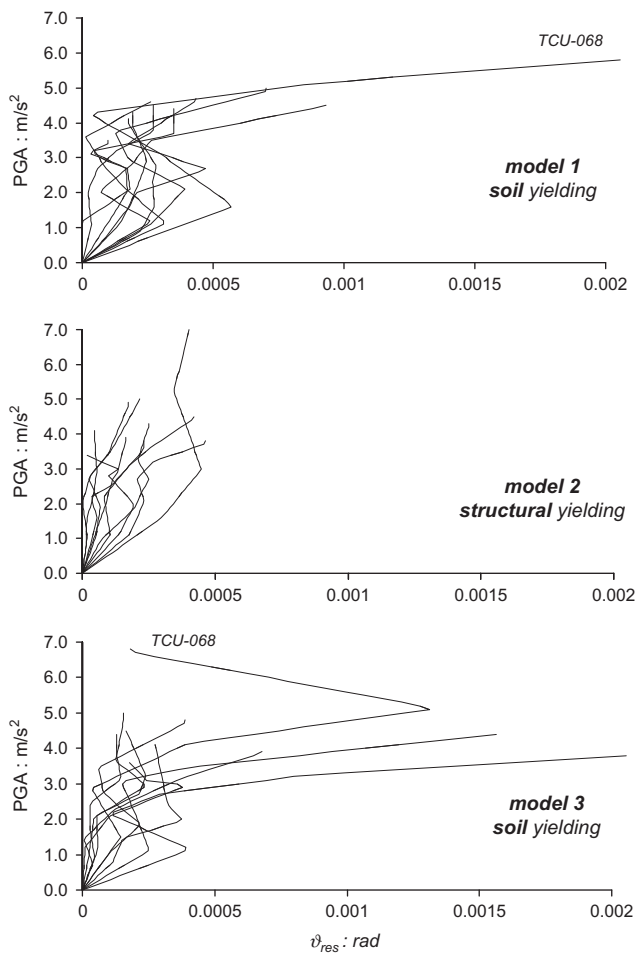


Fig. 18. IDA curves : ϑ_{res} (residual caisson rotation) versus the free-field PGA for the three models.

generally develops smaller displacements, its corresponding rotations as well as yield displacement u_y are also significantly decreased. The net effect was a trend towards larger displacement ductility demands. The opposite statements are true for the *under-designed* foundations—the maximum displacements were larger, but the rotations and the yield displacements are also increased, resulting in a trend towards smaller displacement ductility demands. The fractile curves in Fig. 15 highlight once again the exceptional performance of the *under-designed* lightly loaded *model 1*, exhibiting minimal structural distress, as opposed to the largest demands experienced by its *over-designed* counterpart (*model 2*).

Figs. 16–19 present the IDA curves for the maximum and the residual caisson rotation, θ_{max} and θ_{res} . The latter, θ_{res} , is determined at the end of each dynamic calculation, which, in all analyses, is continued for 5 s after the main motion has ended in order to establish an equilibrium state. The performance does not seem to deviate from any rational intuitive expectation: the seismically *under-designed* caissons demonstrate substantially larger rotations than the *over-designed* counterpart, as a result of the intense caisson–soil interface separation, gapping and soil inelastic action. Notice again the tremendous demand imposed by the large velocity pulse (2.6 m/s) of huge duration (6.3 s) of the

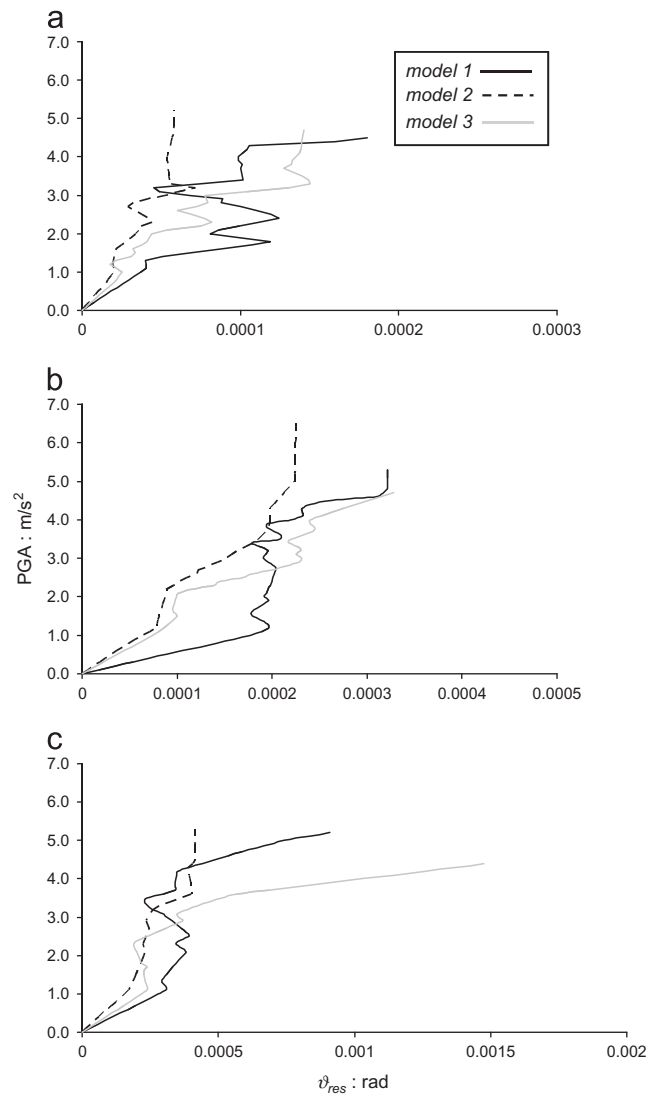


Fig. 19. Summarized IDA curves : ϑ_{res} (residual caisson rotation) for the three models: (a) 16% fractiles, (b) 50% fractiles, (c) 84% fractiles.

TCU-068 record on the *under-designed* caissons, causing global instability and system failure of the lightly loaded *model 1* at $PGA=0.7$ g. Nevertheless, it is remarkable that with the exception

of the performance under the TCU record at high PGA levels (which incidentally are 2 times higher than the actual record), the *under-designed* caissons can avoid collapse sustaining rather

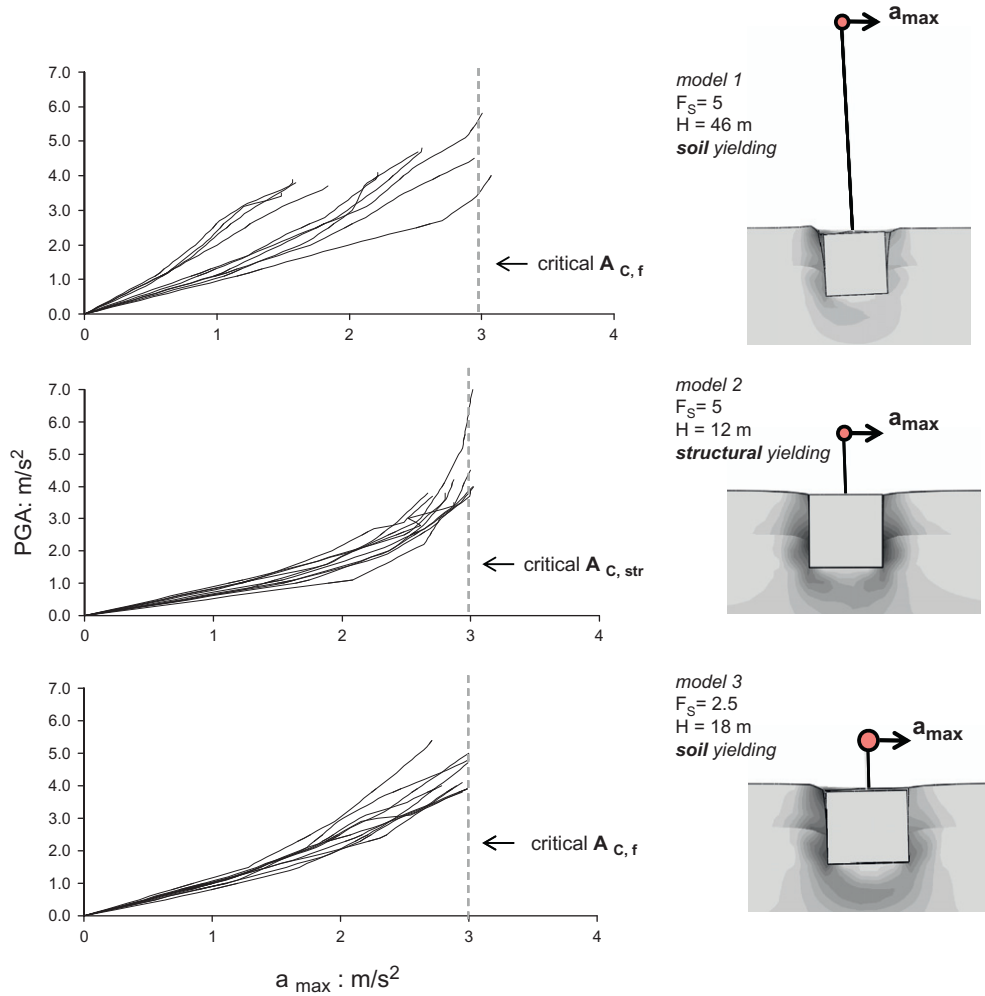


Fig. 20. IDA curves of a_{max} (maximum acceleration at the structure mass) for the three models.

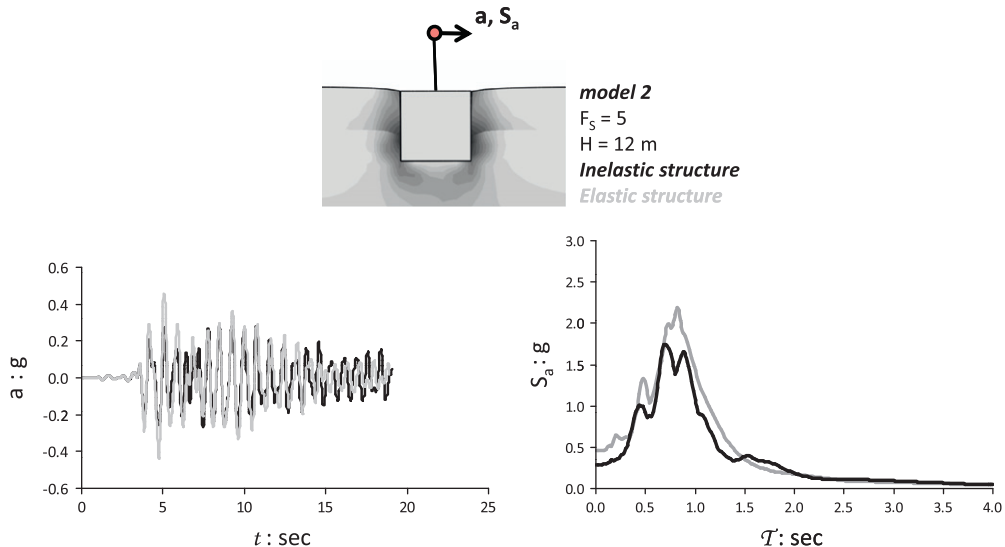


Fig. 21. Acceleration time-histories and “floor” response spectra comparison at the mass level for the *over-designed* *model 2* considering (a) inelastic and (b) elastic superstructure. Record: JMA-000, scaled at *free-field* $PGA=0.4$ g.

tolerable rotations and displacements. This observation is consistent with the results presented by the authors in [49], in which it was shown that in the *over*-designed foundations the developed *drift* is mainly due to flexural distortion, whereas in the *under*-designed ones the *drift* is mainly due to foundation rotation.

Worthy of note are the irregularities exhibited in the IDA curves for the θ_{res} in the *under*-designed caissons, as depicted in Figs. 18–19. Observe the instabilities followed by regain at higher levels, consistent with the variability of the response as a function of the individual records, but especially with the random nature of this EDP.

5.1. IDA curves of maximum acceleration at mass level

In Fig. 20 the comparison is performed for the maximum acceleration at mass level as the Earthquake Demand Parameter. It is immediately evident that all systems exhibit a threshold at $a_{max} \approx 0.3$ g. However, the mechanisms for this acceleration *cut-off* differ with respect to the seismic safety factor of the foundation:

(a) In the *under*-designed foundations, it is the geometric non-linearities and soil inelasticity that dominate the response

and control the value that cannot be exceeded by the transmitted seismic force thus providing a type of seismic isolation for the superstructure ($A_{C,r}=0.3$ g).

(b) In the *over*-designed foundation it is the structural inelasticity that sets an acceleration plateau at $A_{C,str}=0.3$ g, stemming from the bending moment capacity at the base of the column.

The results once again emphasize the favorable performance exhibited by the *under*-designed caissons in terms of structural demand, which become more prominent when combined with a conservative *static* design: for a given PGA level, smaller accelerations are transmitted to the *under*-designed lightly loaded *model 1* than the other two systems.

To further elucidate the effect of structural inelasticity on the seismic response, Fig. 21 compares the acceleration time-histories and the corresponding “floor” response spectra at the mass level of the *over*-designed *model 2* considering both elastic and inelastic superstructure. Excitation: JMA-000 record, down-scaled at a *free-field* PGA=0.4 g, is used. As expected, an elastic superstructure allows a large inertia force to develop at the mass, whereas column inelasticity provides a *cut-off* for the transmitted accelerations.

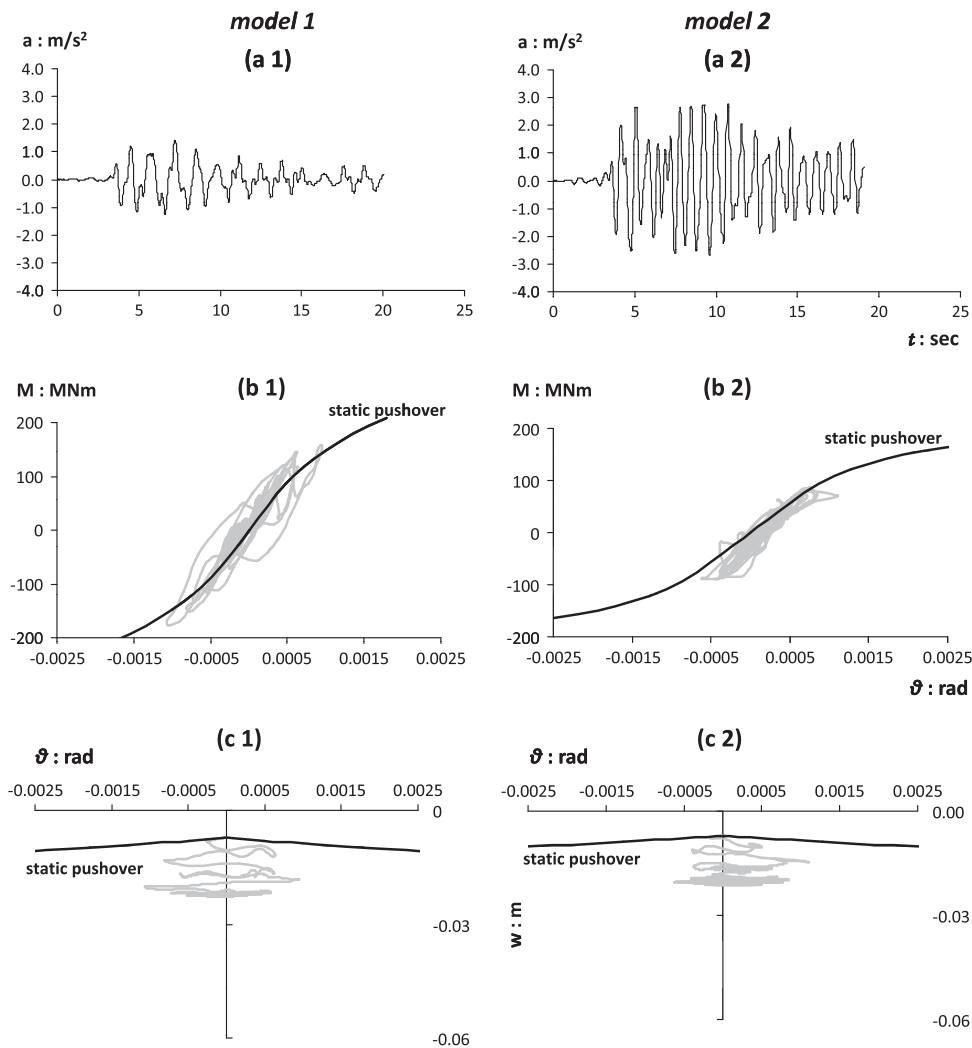


Fig. 22. Typical dynamic response comparison for the systems with $F_s=5$ (light structure) in terms of (a) acceleration time-history at the mass level, (b) moment–column base rotation, (c) caisson settlement–column base rotation. (1) Under-designed foundation, (2) Over-designed foundation. Record: JMA-000, scaled at free-field PGA=0.4 g.

5.2. Some detailed results of dynamic analysis

To get a detailed insight into the nonlinear response mechanisms, typical results of the analyses are portrayed in Figs. 22 and 23 in terms of acceleration time-histories at the mass level, and moment–rotation and settlement–rotation loops at the head of the caisson. Shaking: JMA-000 record, down-scaled at a *free-field* PGA=0.4 g.

The strong contribution of geometric nonlinearities in de-amplifying the seismic motion is again evident in both the lightly and the heavily loaded systems (Figs. 22a1 and 23a3). Yet, intense interface gapping does not provide only a threshold for the transmitted accelerations to the superstructure, but also affects

the frequency content of the motions: note the long-period motions calculated at the structures founded on the *under-designed* caissons (*models* 1 and 3) as opposed to the higher-frequency motion developed at the *over-designed* *model* 2 (Fig. 22a2).

The moment–rotation ($M-\theta$) curves at caisson head for $F_S=2.5$ and $F_S=5.0$ are presented in Figs. 22b1,b2 and 23b3 respectively. $P-\delta$ effects were considered in the calculations. Respecting their design principles, the *over-designed* foundation (*model* 2) experiences limited inelasticity, while the *under-designed* ones (*models* 1 and 3) behave strongly inelastic. Once more, the advantageous contribution of the interface (Figs. 22b1–23b3) rather than the material (Fig. 22b2) and structural nonlinearities in damping the seismic energy is apparent. The shape of the loops in Figs. 22b1 and 23b3 reflects the successive detachments/re-attachments of the caisson from the surrounding soil. Another noteworthy observation from the $M-\theta$ loops of both heavily and lightly loaded structures is that they do not exhibit significant strength degradation, indicating minor $P-\delta$ effects.

However, this favorable performance is not attainable at zero cost: in this case an increase of foundation settlements is expected. Studying the settlement–rotation ($w-\theta$) response of the seismically *over-* and *under-designed* caissons for $F_S=5$ (“light” superstructure), presented in Fig. 22c1,c2, the *over-designed* caisson experiences practically elastic settlement $w \approx 2$ cm. Remarkably, the *under-designed* alternative experiences only marginally larger and quite tolerable seismically induced settlement, $w \approx 2.5$ cm and minimal residual rotation.

As anticipated, the heavily loaded ($F_S=2.5$) *model* 3 exhibits larger accumulated settlements than the lightly loaded counterparts: $w \approx 5.5$ cm, as portrayed in Fig. 23c3. An interesting observation that may be extracted from the ($w-\theta$) loops is that the low F_S system not only sustains larger residual rotations than the high F_S systems, but also the forward directivity pulse carried by the JMA record determines its response.

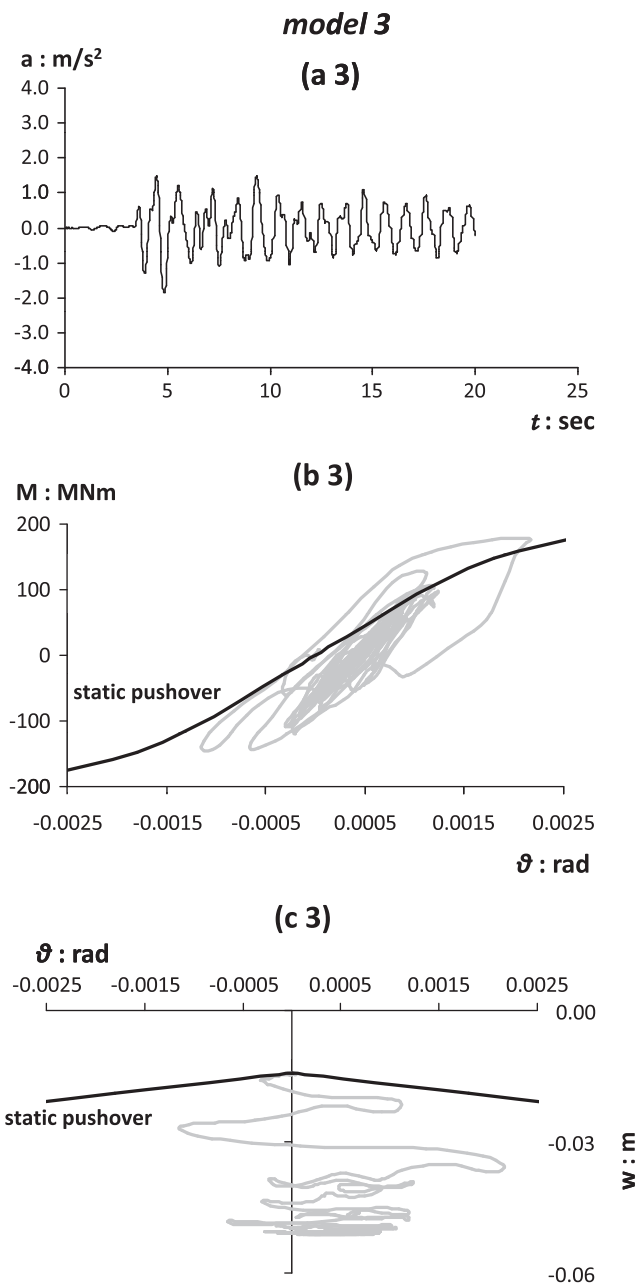


Fig. 23. Typical dynamic response comparison for the under-designed heavily loaded foundation ($F_S=2.5$) in terms of (a) acceleration time-history at the mass level, (b) moment–column base rotation, (c) caisson settlement–column base rotation. Record: JMA-000, scaled at free-field PGA=0.4 g.

6. Summary and conclusions

The present study compares the dynamic response of seismically *over-* and seismically *under-designed* caisson foundations and evaluates the effect of the nonlinear phenomena developed below ground surface on the seismic demand of the superstructures. SDOF structures of varying mass weight, simulating heavily or lightly loaded structures founded through similar rigid cubic caissons on a 2-layer soil stratum are used as examples. The investigation is performed considering soil and structural non-linearity through 3D finite element incremental dynamic analysis (IDA). An ensemble of 10 earthquake motions ranging from medium intensity to very strong, scaled at different PGAs of ground surface motion, was used as base excitation. IDA curves were generated for the maximum horizontal drift, the maximum global ductility demand, the maximum caisson rotation and the residual caisson rotation. The maximum acceleration developed at the superstructure mass was introduced as an ad hoc Engineering Demand Parameter.

From the study, the following conclusions could be inferred:

- In terms of structural distress, there is a distinct predominance in the performance of the structures founded on the *under-designed* caissons (*models* 1 and 3) developing significantly reduced horizontal drifts and ductility demands, as opposed to the one founded on the *over-designed* caisson; clear evidence

that the mechanism of interface nonlinearities acts as a “fuse” for the superstructure.

- Concerning the accelerations developed at the structure mass level, both mechanisms of geometric nonlinearities and structural inelasticity, prevalent in the response of the seismically *under-* and *over-*designed foundations respectively, provide a plateau for the maximum transmitted accelerations. Due to the strongly nonlinear soil–structure interaction effects present in the former mechanism, however, the superstructure experiences a longer-period motion as compared to the one filtered by the localized plasticity in the column.
- In terms of system performance, the *under-*designed foundations experienced increased dynamic settlements and rotations as compared to the *over-*designed one. Strikingly, however, they sustained only minimal residual displacements and tilting, owing much to the massive weight of the caisson which acts as a restoring force.

Overall, the study highlighted the efficacy of *under-*designed caisson foundations with high static factor of safety, providing a low-cost foundation solution with a high seismic isolation potential.

Acknowledgments

A. Zafeirakos acknowledges the financial support from the European Union (European Social Fund – ESF) and Greek national funds through the Operational Program “Education and Lifelong Learning” of the National Strategic Reference Framework (NSRF) – Research Funding Program: *Heracleitus II*. Investing in knowledge society through the European Social Fund.

N. Gerolymos and V. Drosos acknowledge financial support from the research project “DARE” funded by the European Research Council’s Programme “Ideas” in support for Frontier Research, under Contract number ERC-2008-AdG 228254-DARE.

References

- [1] ABAQUS, Inc. ABAQUS analysis user's manual, VERSION 6.8, Providence, RI, USA; 2008.
- [2] Anastasopoulos I, Gazetas G, Loli M, Apostolou M, Gerolymos N. Soil failure can be used for seismic protection of structures. *Bulletin of Earthquake Engineering* 2010;8:309–26.
- [3] Bertero VV. Strength and deformation capacities of buildings under extreme environments. In: Pister KS, editor. *Structural engineering and structural mechanics*. Englewood Cliffs, NJ: Prentice Hall; 1977. p. 211–5.
- [4] Borja RI, Wu WH, Smith HA. Nonlinear response of vertically oscillating rigid foundations. *Journal of Geotechnical and Geoenvironmental Engineering*, ASCE 1993;119(5):893–911.
- [5] Borja RI, Wu WH, Amies AP, Smith HA. Nonlinear lateral, rocking, and torsional vibrations of rigid foundations. *Journal of Geotechnical and Geoenvironmental Engineering*, ASCE 1994;94(3):491–513.
- [6] Chatzigogos CT, Figini R, Pecker A, Salençon J. A macroelement formulation for shallow foundations on cohesive and frictional soils. *International Journal for Numerical and Analytical Methods in Geomechanics* 2011;35(8):902–31.
- [7] Dominguez J. Dynamic stiffness of rectangular foundations. *Research report R78-20*, MIT; 1978.
- [8] Elsabee F., Morray J.P. Dynamic behavior of embedded foundations. *Research report R77-33*. MIT; 1977.
- [9] Figini R, Paolucci R, Chatzigogos CT. A macro-element model for non-linear soil–shallow foundation–structure interaction under seismic loads: theoretical development and experimental validation on large scale tests. *Earthquake Engineering & Structural Dynamics* 2012;41(3):475–93.
- [10] Gajan S, Kutter BL, Phalen JD, Hutchinson TC, Martin GR. Centrifuge modeling of load–deformation behavior of rocking shallow foundations. *Soil Dynamics and Earthquake Engineering* 2005;25:773–83.
- [11] Garini E, Gazetas G. Destructiveness of earthquake ground motions: intensity measures versus sliding displacement. In: *Proceedings of 2nd international conference on performance-based design in earthquake geotechnical engineering*, May 28–30, 2012, Taormina, Italy. p. 886–99.
- [12] Gazetas G. Analysis of machine foundation vibrations: state of the art. *Soil Dynamics and Earthquake Engineering* 1983;2:2–42.
- [13] Gazetas G. Simple physical methods for foundation impedances. In: Benerjee PK, Butterfield R, editors. *Dynamics of Foundations and Buried Structures*. Elsevier Applied Science; 1987. p. 44–90 [Chapter 2].
- [14] Gazetas G, Apostolou M, Anastasopoulos I. Seismic uplifting of foundations on soft soil, with examples from Adapazari (Izmit 1999, Earthquake). *Foundations: Innovations, Observations, Design & Practice*. British Geotechnical Association 2003:37–50.
- [15] Gelagoti F, Kourkoulis R, Anastasopoulos I, Gazetas G. Rocking isolation of low-rise frame structures founded on isolated footings. *Earthquake Engineering & Structural Dynamics* 2012;41(7):1177–97.
- [16] Gerolymos N, Gazetas G. Winkler model for lateral response of rigid caisson foundations in linear soil. *Soil Dynamics and Earthquake Engineering* 2006;25(5):347–61.
- [17] Gerolymos N, Gazetas G. Development of Winkler model for static and dynamic response of caisson foundations with soil and interface nonlinearities. *Soil Dynamics and Earthquake Engineering* 2006;26(5):363–76.
- [18] Gerolymos N, Gazetas G. Static and dynamic response of massive caisson foundations with soil and interface nonlinearities—validation and results. *Soil Dynamics and Earthquake Engineering* 2006;26(5):377–94.
- [19] Gerolymos N, Giannakou A, Anastasopoulos I, Gazetas G. Evidence of beneficial role of inclined piles: Observations and summary of numerical analyses. *Bulletin of Earthquake Engineering* 2008;6(4):705–22.
- [20] Gerolymos N, Drosos V, Gazetas G. Seismic response of single-column bent on pile: evidence of beneficial role of pile and soil inelasticity. *Bulletin of Earthquake Engineering* 2009;7(2):547–73.
- [21] Giannakou A, Gerolymos N, Gazetas G, Tazoh T, Anastasopoulos I. Seismic behavior of batter piles: elastic response. *Journal of Geotechnical and Geoenvironmental Engineering*, ASCE 2010;136(9):1187–99.
- [22] Harden CW, Hutchinson TC. Beam-on-nonlinear-Winkler-foundation modeling of shallow, rocking-dominated footings. *Earthquake Spectra* 2009;25(2):277–300.
- [23] Hutchinson TC, Boulanger RW, Chai Y.H., Idriss I.M. Inelastic seismic response of extended pile shaft supported bridge structures. *PEER Report 2002/14*. Department of Civil and Environmental Engineering University of California, Irvine, Department of Civil and Environmental Engineering University of California, Davis.
- [24] Ishibashi I, Zhang X. Unified dynamic shear moduli and damping ratios of sand and clay. *Soils & Foundations* 1993;33(1):12–191.
- [25] Kausel E. Forced vibrations of circular foundations on layered media. *Research Report R74-11*. MIT; 1974.
- [26] Kausel E, Roesset JM. Dynamic stiffness of circular foundations. *Journal of the Engineering Mechanics Division*, ASCE 1975;101(6):770–85.
- [27] Kawashima K, Nagai T., Sakellaraki D. Rocking seismic isolation of bridges supported by spread foundations. In: *Proceedings of the 2nd Japan–Greece workshop on seismic design, observation, and retrofit of foundations*, Tokyo, Japan; April 3–4, 2007. p. 254–65.
- [28] Lam IP, Chaudhury D. Modeling of drilled shafts for seismic design. *NCEER Report I12D-2.5*. The National Center for Construction Education and Research; 1997.
- [29] Lignos DG, Krawinkler H, Whittaker AS. Prediction and validation of sidesway collapse of two scale models of a 4-story steel moment frame. *Earthquake Engineering and Structural Dynamics* 2011;40(7):807–25.
- [30] Luco JE, Westman RA. Dynamic response of circular footings. *Journal of the Engineering Mechanics Division*, ASCE 1971;97(5):1381–95.
- [31] Luco N, Cornell CA. Effects of connection fractures on SMRF seismic drift demands. *Journal of Geotechnical and Geoenvironmental Engineering*, ASCE 2000;126:127–36.
- [32] Mergos PE, Kappos AJ. Seismic damage analysis including inelastic shear–flexure interaction. *Bulletin of Earthquake Engineering* 2010;8:27–46.
- [33] Mita A, Luco JE. Dynamic response of a square foundation embedded in an elastic halfspace. *Soil Dynamics and Earthquake Engineering* 1989;8(2):54–67.
- [34] Nassar A.A., Krawinkler H. Seismic demands for SDOF and MDOF systems. *Research report No. 95*. The John A. Blume Earthquake Engineering Center, Stanford University; 1991.
- [35] Novak M, Beredugo YO. Vertical vibration of embedded footings. *Journal of the Soil Mechanics and Foundations Division*, ASCE 1972;98(SM12):1291–310.
- [36] Paolucci R. Simplified evaluation of earthquake induced permanent displacement of shallow foundations. *Journal of Earthquake Engineering* 1997;1(3):563–79.
- [37] Panagiotidou AI, Gazetas G, Gerolymos N. Pushover and seismic response of foundations on stiff clay: analysis with P – Δ effects. *Earthquake Spectra* 2012;28(4):1589–618.
- [38] Pecker A. Capacity design principles for shallow foundations in seismic areas. In: *Proceedings of the 11th European conference on earthquake engineering*; 1998. p. 303–16.
- [39] Pecker A. A seismic foundation design process, lessons learned from two major projects: the Vasco de Gama and the Rion Antirion bridges. In: *ACI international conference on seismic bridge design and retrofit*, University of California at San Diego, La Jolla, USA; 2003.
- [40] Pecker A, Chatzigogos C.T.. Non linear soil structure interaction: impact on the seismic response of structures. *Geotechnical, Geological, and Earthquake Engineering* (17); 2010: 79–103 [Earthquake Engineering in Europe].
- [41] Suarez V, Kowalsky MJ. Displacement-based seismic design of drilled shaft bents with soil–structure interaction. *Journal of Earthquake Engineering* 2007;11(6):1010–30.

- [42] Tajirian FF, Tabatabaie M. Vibration analysis of foundations in layered media. *Vibration Problems in Geotechnical Engineering*, ASCE 1985:27–46.
- [43] Tassoulas J.L. Elements for the numerical analysis of wave motion in layered media. Research report R81-2. MIT; 1981.
- [44] Vamvatsikos D, Cornell CA. Incremental dynamic analysis. *Earthquake Engineering and Structural Dynamics* 2002;31(3):491–514.
- [45] Vamvatsikos D, Cornell CA. Applied incremental dynamic analysis. *Earthquake Spectra* 2004;20(2):523–53.
- [46] Vamvatsikos D, Cornell CA. Tracing and post-processing of IDA curves: theory and software implementation. Report No. RMS-44, RMS Program, Stanford University, Stanford; 2001.
- [47] Varun, Assimaki D, Gazetas G. A simplified model for lateral response of large diameter caisson foundations-linear elastic formulation. *Soil Dynamics and Earthquake Engineering* 2009;29(2):268–91.
- [48] Vetetsos AS, Wei YT. Lateral and rocking vibration of footings. *Journal of the Soil Mechanics and Foundations Division, ASCE* 1971;97:1227–48.
- [49] Zafeirakos A, Gerolymos N, Gazetas G. The role of soil and interface nonlinearities on the seismic response of caisson supported bridge piers. In: *Proceedings of the 5th international conference on geotechnical earthquake engineering*, Santiago, Chile; 2011.